Localization of light: beginning of a new optics

E. Jimenez-Villar, M. C. S. Xavier, J. G. G. S. Ramos, N. U. Wetter, Valdeci Mestre, et al.

E. Jimenez-Villar, M. C. S. Xavier, J. G. G. S. Ramos, N. U. Wetter, Valdeci Mestre, Weliton S. Martins, Gabriel F. Basso, Victor A. Ermakov, Francisco Chagas Marques, Gilberto F. de Sá, "Localization of light: beginning of a new optics," Proc. SPIE 10549, Complex Light and Optical Forces XII, 1054905 (22 February 2018); doi: 10.1117/12.2288993

SPIE.

Event: SPIE OPTO, 2018, San Francisco, California, United States

Localization of light: Beginning of a new optics

E. Jimenez-Villar*[a,b], M.C. S. Xavier[c,d], J.G.G.S. Ramos[d], N. U. Wetter[a], Valdeci Mestre[e], Weliton S. Martins[f], Gabriel F. Basso[g], Victor A. Ermakov[b], Francisco Chagas Marques[b], Gilberto F. de Sá[h]
[a]Instituto de Pesquisas Energéticas e Nucleares, CNEN_IPEN, Rua Prof. Lineu Prestes 2242− Cidade Universitária, São Paulo, SP, Brazil 05508-000; [b]Departamento de Física aplicada, IFGW, Universidade Estadual de Campinas, Campinas, SP, Brazil 13083-859; [c]Departamento de Física, Universidade Estadual da Paraíba, Araruna, PB, Brazil 58233-000; [d]Departamento de Física, Universidade Federal da Paraiba, Joao Pessoa, PB, Brazil 58051-970; [e]CCEA, Universidade Estadual da Paraíba, Patos, PB, Brazil 58706-560; [f]Departamento de Física, Universidade Federal Rural de Pernambuco, Recife, PE, Brazil 52171-900; [g]Departamento de Informatica, Universidade Federal da Paraiba, Joao Pessoa, PB, Brazil 58051-970; [h]Departamento de Química Fundamental, Universidade Federal de Pernambuco, Recife, PE, Brazil 50670-901
Ernesto.Jimenez@uv.es

ABSTRACT

In recent years, there has been a dramatic progress in the photonics field of disordered media, ranging from applications in solar collectors, photocatalyzers, random lasing, and other novel photonic devices, to investigations into fundamental topics, such as localization of light and other phenomena involving photon interactions. Anderson localization of light is an open researcher frontier, which has greatly attracted the attention of researchers in the past few decades. In this work, we study the transport of light in a strongly disordered optical medium composed by core-shell nanoparticles (TiO_2@Silica) suspended in ethanol solution. We demonstrate the crossover from a diffusive transport to a localization transition regime as TiO_2@Silica nanoparticle concentration is increased. A striking phenomenon of enhanced absorption, mainly near the input border, arises at the localization transition, from which an increase of refractive index was inferred. An increase of the density of localized states and absorption near the input border is reported when the incidence angle is increased. The specular reflection, measured for the photons that enter the sample, is considerably lower than the effective internal reflection undergone by the coherently backscattered photons in the exact opposite direction, indicating a non-reciprocal propagation of light (parity-symmetry breaking). A theoretical simulation, performed through random-matrix theory, agrees satisfactorily with the experimental results, showing the generality of this approach to address transport phenomena.

Keywords: Anderson localization of light, photonic in disordered media, core-shell nanoparticle, enhanced absorption, non-reciprocation of light, random-matrix theory.

1. INTRODUCTION

There has been growing interest in disordered optical media in recent years, due to their potential applications in photovoltaics cell [1], random laser [2–4], localization of light [5], etc. Anderson localization is one of the most interesting phenomena in solid-state physics. Particularly, localization of light is an open research frontier which, besides being a fundamental topic, also could present significant applications. Considering that localization is a wave (interferential) phenomenon, Sajeev john and Anderson himself extended this idea to optics [5–8]. Optics seems an ideal framework to study localization and associated phenomena, due to the (seemingly) non-interacting nature of photons. In fact, various pioneering experiments that studied the transmission of electromagnetic waves through strongly disordered media have claimed the observation of Anderson localization of light [9–11]. However, these works have been questioned [12–15]. The inelastic scattering processes (residual absorption or nonlinearity) can lead to a decrease in the photon coherence length, hampering the interference effects (localization). Indeed, according to the theoretical prediction of Sajeev John and our previous experimental results [16], an enhanced absorption arises when the system approaches localization. Localization of light has become in very confuse topic. This may be because it has been frequently addressed as a conventional, exclusively interferential phenomenon in classical cavities, which is inappropriate. Localization of light is a special interferential phenomenon of electromagnetic waves in chaotic cavities, which must lead to a strong photon correlation [8].

Complex Light and Optical Forces XII, edited by Enrique J. Galvez, David L. Andrews, Jesper Glückstad, Proc. of SPIE Vol. 10549, 1054905 · © 2018 SPIE
CCC code: 0277-786X/18/$18 · doi: 10.1117/12.2288993

This statistical problem at the mobility edge in a 3D system was addressed for the first time by Altshuler et al. in strongly disordered electronic media [17]. An extended review about the localization phenomenon, published by Mirlin, can be found elsewhere [18]. In this work, we report several pieces of experimental evidence of localization of light in a colloidal suspension of TiO_2@Silica nanoparticles (NPs) in an ethanol solution. By using a Stöber method [19], TiO_2 NPs were coated with a homogeneous silica shell of ~40 nm thickness. In order to eliminate the residues of the chemical synthesis and, consequently, to reduce residual absorption, subsequent dialysis and centrifugation processes were performed. The silica coating with thicknesses around or above 40 nm prevents the "optical" junction of the TiO_2 scattering surfaces (steric "optical" effect) [20], decreasing the near-field coupling that could hamper localization [21]. We called this property optical colloidal stability [20]. Additionally, the silica shell provides a light-coupling enhancement with TiO_2 scattering cores [22], inertness [23,24], and high dispersibility [25–30], which has enabled their use in numerous applications [31–35]. A striking phenomenon of enhanced absorption is observed when the system approaches localization, from which an increase of the effective refractive index was proposed. This enhancement of absorption and refractive index was interpreted as that localized photons interact several times with the same particles, molecules or atoms within the localized states. The last phenomenon must be more pronounced near the input border, due to the increase of localization in the vicinity of the sample boundary for an internal reflection >0 at the input border as was theoretically predicted by Mirlin in disordered electronic media [18,36]. The enhancement of the effective refractive index near the sample input border (n_{eff0}) by localization (successive elastic polarization of valence electrons to virtual states) finds a parallel in the dynamic barrier proposed by Campagnano and Nazarov [37] in the border of a disordered electronic medium. This n_{eff0} increase implies that an increase of the incidence angle would provoke a large increase of the internal reflection, which in turn, must force the photons path to be longer (near the input border). Consequently, the likelihood of interference (near the input border) should increase. This issue was addressed theoretically by Ramos and co-workers [38], who demonstrated that the presence of a finite barrier (internal reflection>0) at the border provokes an increase of the quantum interference in a disordered electronic medium (localization increase). In this work, measurements of absorption, absorption near the input border, photon cloud propagation as a function of NPs concentration and the incidence angle and coherent backscattering were performed in the TiO_2@Silica colloidal suspension. In parallel, by random-matrix theory (theoretical simulation), we determined the conductance as a function of the effective internal reflection felt by the coherently backscattered photons (previously localized photons), showing satisfactory agreement with the experimental results. Random-matrix theory has seen a revival of interest in past decades, which has been applied to a variety of physical phenomena [39,40]. The discovery of a relation between universal properties of large random matrices and universal conductance fluctuations in disordered conductors has led to the development of a random-matrix theory of quantum transport [17,41]. In atomic physics, Wigner showed that the properties of an atomic core depend on the sample in a seemingly random way. Despite the randomness, Wigner perceived that in generic quantum systems, statistic properties as the mean and variance are universal, i.e. these quantities depend on fundamental symmetries. In turn, Wigner inferred that despite the randomness of the Hamiltonians H, these obey symmetry relations linked to the time-reversal and spin rotation symmetries. The open quantum systems can be descripted by scattering matrices S that are related to the Hamiltonian in the scattering region through the Mahaux-Weidenmuller formula, equation (1).

$$S = 2\pi i W(E - H - i\pi W^{\dagger}W)^{-1}W^{\dagger} \tag{1}$$

The S matrix links input and output channels, so it has a dimension equal to the total number of channels. The H matrix has a dimension equal to the number of resonances in the scattering region. The number of resonances is directly related to the size of the scattering region. The W matrix links open channels to the resonances. Thus, the W matrix reveals the coupling or the tunneling rates between the two different regions in the coordinate space. In turn, the scattering matrix can be written in terms of sub-blocks of transmission t and reflection r. Notice that, the three fundamental symmetries, incorporated in the Hamiltonian, that identify (i) systems with time-reversal (Gaussian orthogonal ensemble), (ii) systems without time-reversal (Gaussian unitary ensemble) and (iii) systems without spin-rotation (Gaussian symplectic ensemble) are also directly identified in the scattering matrix. The transport properties can be obtained through the transmission block t from S matrix, such that the conductance is written as:

$$g = \mathbf{tr}(tt^{\dagger}) \tag{2}$$

In this way, the conductance belongs to one of the three ensembles of Wigner-Dyson. In this paper, we used an ensemble with several H realizations, showing that the theoretical simulation agrees very well with the experimental results, which reveals that the disordered optical systems are also universals.

2. MATERIALS AND METHODS

Samples preparation: TiO_2@Silica NPs, synthesized by an improved Stöber method [16,19], were dispersed in ethanol solution at [NPs] of 14, 47, 70, 140 and 280 x10^{10} NPs ml^{-1}.
Absorption experiment: For each [NPs], the macroscopic absorption length (l_{MA}) was determined from the exponential decay of the transmitted intensity $\left(I_{TC}(d) \propto e^{-d/l_{MA}}\right)$ for large d using a very small solid detection angle (pulsed Nd:Yag laser, 532 nm) [16].
Propagation experiment: For [14x10^{10} NPs ml^{-1}] (diffusive regime) and [140x10^{10} NPs ml^{-1}] (localization), the intensity profile $I(x,y)$ of a Gaussian probe beam (He-Ne laser) was measured as a function of the incidence angle after propagating a distance d≈2.3 mm through the scattering medium. A CCD camera collected the image of the profile at the sample output face. The diameter of the input probe beam is <100 μm full-width at half-maximum (FWHM), which correspond to approximately 3x10^3 channels or terminals.
Backscattering experiment: For the measurement of coherent backscattering, the sample is illuminated through a beam splitter that reflects 50% of the laser intensity and with a perpendicular polarization to the incidence plane. The light backscattered is collimated by a lens L_3 (25 mm focal length) and a CCD collects it [16,42].
Theoretical simulation: We perform a theoretical simulation with an ensemble of N=5x10^5 Hamiltonians. The statistical properties of the conductance g naturally arise with an error of order to N^{-1}. In order to simulate the experimental conditions (monochromatic He-Ne laser), we considered a single energy per terminal. The g conductance is computed as a function of the effective internal reflection felt by the coherently backscattered photons (backscattering terminal). We simulate both the universal orthogonal ensemble (with time-reversal symmetry) and the unitary ensemble (without time-reversal symmetry). It is known that, systems without time reversal symmetry do not lead to quantum interference, such that the only significant contribution are the classical paths, also known as difusons. Instead, the orthogonal ensembles preserve the time-reversal symmetry, and a perturbative expansion of conductance (ergodic regime) leads to both terms: the direct term (difusons) and the term associated to the quantum interference (localized states), also known as cooperons. We develop a strategy to compute separately the interference terms, which consists in the subtraction of the unitary term to the conductance value calculated with the orthogonal ensemble. The mean over each ensemble were computationally calculated.

3. RESULTS AND DISCUSSION

3.1 Absorption measurement

In order to determine the macroscopic absorption length (l_{MA}), the transmitted intensity ($I_{TC}(d;\theta)$) was measured as a function of slab thickness for large d using a very small solid detection angle. l_{MA} can be determined from the inverse slope (log scale) of exponential decay $\left(e^{-d/l_{MA}}\right)$, where l_{MA} can be expressed as $l_{MA} \propto (l_T \times l_{In})^{1/2}$ and, l_T and l_{In} are the transport and inelastic mean free path, respectively [43].

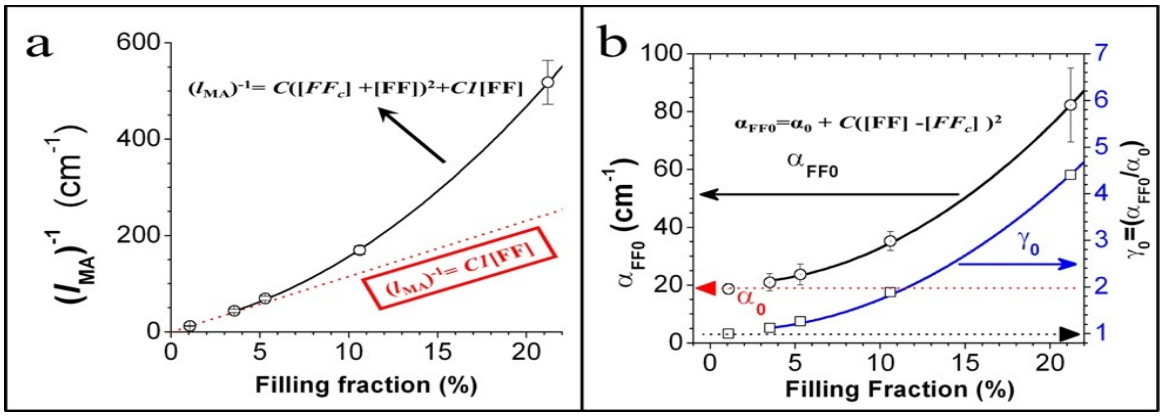

Figure 1. Absorption measurement: a) Inverse of the macroscopic absorption length $(l_{MA})^{-1}$ as a function of the filling fraction. The red dotted line represents the expected behavior in the diffusive regime (C1[FF]). The black solid line represents the fit with the function $C([FF]-[FF_c])^2 + C1[FF]$. b) Anomalous increase of: α_{FF0} (left) and the γ_0 (right) as [FF] is increased, the red dotted line represents the α_0 value. Error bars correspond to fitting errors.

Figure 1a shows $(l_{MA})^{-1}$ values as a function of filling fraction, [FF]. As can be observed, $(l_{MA})^{-1}$ increases more quickly than the expected linear increase, which represents an anomalous behavior. Notice that if l_T and l_{In} would be inversely proportional to [Nps] or [FF], a $(l_{MA})^{-1} \propto [FF]$ dependence (red dotted line) must be expected. The experimental points have been fitted (black solid line) with the following function: $(l_{MA})^{-1} = C([FF] + [FF_c])^2 + C1[FF]$, where C, C1 are constants and $[FF_c]$ can be interpreted as the critical filling fraction for which starts the l_{MA} anomalous behavior. The linear part (C1[FF]) corresponds to the expected linear increase at the diffusive regime. The quadratic term would represent the enhanced absorption contribution by localization effect. In order to study in depth this anomalous absorption behavior, the microscopic absorption length near the input border (l_{In0}) was determined by the relation $l_{MA} = (l_{T0} \times l_{In0})^{1/2}$ equation, where l_{T0} and l_{In0} are the transport and inelastic mean free path near the input border, respectively. l_{T0} values were determined experimentally in our previous work [16]. $(l_{In0})^{-1}$ per filling fraction (α_{FF0}) is plotted (Fig. 1b, left) as a function of the filling fraction ([FF]). For each [FF], the α_{FF0} values (absorption coefficient) are determined from $\alpha_{FF0} = (l_{In0} \times [FF])^{-1}$. Contrary to expectations, α_{FF0} is not constant; it increases quickly in [FF] as a function $\alpha_{FF0} = \alpha_0 + C([FF]-[FF_0])^2$, where C is a constant, and α_0 and $[FF_0]$ are α_{FF0} at the limit of the diffusive regime and the critical filling fraction which starts the α_{FF0} anomalous increase, respectively. This anomalous increase of the absorption coefficient near the input border for [NPs]≥ [47x10^{10}NPs ml^{-1}] represents a very interesting result, which could be strong evidence for the existence of the photon mobility edge [5,8]. Fig. 1b (right) shows the enhanced absorption factor near the input border (γ_0) determined by the ratio between effective and classical absorption ($\gamma_0 = \alpha_{FF0}/\alpha_0$). This γ_0 parameter could be interpreted such that photons travel an average of γ_0 times around a closed loop path near the input border, i.e. each photon would interact at an average of γ_0 times with the same particles, atoms or molecules within the closed loop paths. This idea could be extrapolated to the elastic polarization of valence electrons to virtual states, which would imply an increase also in the effective refractive index near the input border (n_{eff0}).

3.2 Propagation experiment

For [14x10^{10} NPs ml^{-1}] (diffusive regime) and [140x10^{10} NPs ml^{-1}] (localization), the intensity structure of a Gaussian probe beam (He–Ne laser) was measured as a function of the incidence angle (0º, 30º, 60º, 70º) after propagating a distance d≈2.3 mm through the scattering medium. Figure 2a, b and c show the normalized intensity profiles at the sample output face for the incidence angle of 0º, 60º and 70º. As can be observed, the intensity profiles are not Gaussian, these could be fitted with a $e^{-2\left(|r|/\sigma\right)^{1+\nu}}$ function (red solid line), where r is the radial distance of the beam center and $0<\nu<1$. When the incidence angle is increased, the intensity (profile) decreases more quickly for large r and, for r near zero (cusp) the intensity increases adopting an acute form (discontinuous derivative), i.e. the intensity profile adopts a triangular shape. This effect is notable as the incidence angles is increased and could be caused by an increase of absorption near the input border, which in turn, would be originated by an increase of the density of superficial localized states. Notice that, the intensity for large r must represent those photons with longer paths, which would be those photons previously localized near the input border since localization must increase near the input border [18,36]. The integrated intensity profiles $\left(I(\theta) = \int_{-\infty}^{+\infty} I(x,y)\,dxdy\right)\left(\mathrm{I}(\theta) = \int_{-\infty}^{+\infty} \mathrm{I(x,y)\,dxdy}\right)$ were determined for each incidence angle θ. In figure 2d, $\frac{I(0°)}{I(\theta)}$ ratio, which would represent the relative conductance $G(\infty;\theta)$ for a negligible absorption, are plotted as a function of the incidence angle for [14x10^{10} NPs ml^{-1}] (diffusive regime) and [140x10^{10} NPs ml^{-1}] (localization). For [140x10^{10} NPs ml^{-1}], $I(\theta)$ decreases 1.05, 1.17 and 1.28 times with regard $I(0º)$ for incidence angles of 30º, 60º and 70º, respectively. However, for [14x10^{10} NPs ml^{-1}] (diffusive regime), $I(\theta)$ is insensitive to the incidence angle. For each incidence angle, the confinement of the beam at the output plane is quantified by the inverse participation ratio (equation 3), which has units of inverse area, and an effective width $\omega_{eff} = (P)^{-1/2}$.

$$P \equiv \left[\int I(x,y)^2\,dxdy\right] \Big/ \left[\int I(x,y)\,dxdy\right]^2 = \frac{1}{\pi}\left[\int I(r)^2\,dr\right] \Big/ \left[\int I(r)\,dr\right]^2 \qquad (3)$$

Figure 2e (left) shows ω_{eff} as a function of the incidence angle for [140x10^{10} NPs ml^{-1}] (localization), revealing an ω_{eff} decrease as the incidence angle is increased above 30º. Figure 2e (right) shows the relative effective width with regard to the normal incidence, $\left(\frac{\omega_{eff}(0°)}{\omega_{eff}(\theta)}\right)$ (normalized width). For 30º, ω_{eff} decreases less than 1%, which is within the measurement error. However, a significant ω_{eff} decrease is observed for 60º and 70º. This ω_{eff} decrease is associated to the quicker decay of the intensity profile at large r when the incidence angle is increased. For a negligible absorption, ω_{eff} represents the mean conductance averaged by depth (from 0 up to 2.3 mm). Therefore, if $\frac{\omega_{eff}(0°)}{\omega_{eff}(30°)} \approx 1$, then for 30º,

the asymptotic value of relative conductance for large *depth*→∞, $G(\infty;30^o)$, should be equal to the inverse of the relative conductance at *depth*=0, $(G(0;30^o))^{-1}$. Thus, let us introduce the following conjecture: For an incidence angle θ, the asymptotic value of relative conductance without absorption for large *depth*, $G_{\text{-abs}}(\infty;\theta)$, should correspond with the localization increase at *depth*=0, $(G_{\text{-abs}}(0;\theta))^{-1}$, i.e. $G_{\text{-abs}}(\infty;\theta)=(G_{\text{-abs}}(0;\theta))^{-1}$. This would imply that, for a negligible absorption, the conductance averaged by depth, ω_{eff}, should not change with incidence angle, i.e. a ω_{eff} decrease with the incidence angle would be directly related to an increase of absorption near the input border. This can be interpreted as that, for a negligible absorption, an increase of the density of superficial localized states when the incidence angle increases would induce a similar decrease of the density of localized states for large *depth*. For [$14\text{x}10^{10}$ NPs ml^{-1}] (diffusive regime), ω_{eff} is insensitive to the incidence angle. Therefore, the values of relative conductance, $G(\infty;\theta)$, extracted from this experiment, must be affected by absorption for 60º and 70º (ω_{eff} decrease), which yield inaccurate values. In order to estimate the relative conductance without absorption effects, we introduce another strategy. The ratio of the integrated intensity profile, determined from $r=-{}^{\omega_{\text{eff}}}/_{2}$ up to ${}^{\omega_{\text{eff}}}/_{2}$, $\left(\frac{I_{\text{Cent}}(0^\circ)}{I_{\text{Cent}}(\theta)}\right)$, where $I_{\text{Cent}}(\theta)=\int_{-\omega_{\text{eff}}/2}^{+\omega_{\text{eff}}/2} I(x,y)dxdy$, is scaled by the normalized width $\left(\frac{\omega_{\text{eff}}(0^\circ)}{\omega_{\text{eff}}(\theta)}\right)$. Thereby, the relative conductance without absorption, $G_{\text{-abs}}(\infty;\theta)$, was estimated by the expression $G_{-\text{abs}}(\infty;\theta)\approx\frac{I_{\text{Cent}}(0^\circ)}{I_{\text{Cent}}(\theta)}\times\frac{\omega_{\text{eff}}(0^\circ)}{\omega_{\text{eff}}(\theta)}$.

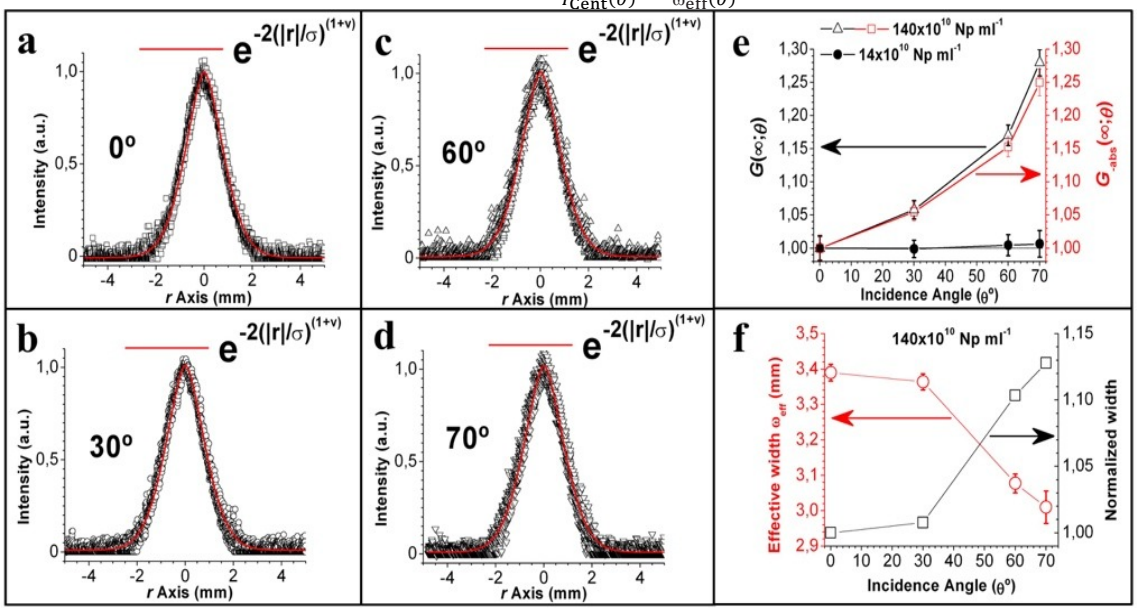

Figure 2. Normalized intensity profiles for incidence angles of: a) 0º, b) 30º, c) 60º and d) 70º. The intensity profiles are fitted to $e^{-2\left(|r|/\sigma\right)^{1+\nu}}$ (red solid lines), where 0<ν<1. e) For [NPs] of [$140\text{x}10^{10}$ NPs ml^{-1}] (localization), increase of $G(\infty;\theta)$ (left, black triangles) and $G_{\text{-abs}}(\infty;\theta)$ (right, red square) as angle of incidence increases, and for [$14\text{x}10^{10}$ NPs ml^{-1}] (diffusive regime), $G(\infty;\theta)$ (left, black dots) remain constant as the incidence angle is increased. f) For [$140\text{x}10^{10}$ NPs ml^{-1}], ω_{eff} decrease (left, red circles) and the increase normalized width $\left(\frac{\omega_{\text{eff}}(0^\circ)}{\omega_{\text{eff}}(\theta)}\right)$ (right, black squares) as the incidence angle is increased.

In the above experiments, we show an increase of relative conductance and infer an increase of localization near the input border as the incidence angle is increased. This fact was associated to an increase of the density of localized states near the input border, which was attributed to a large increase of the internal reflection (input border) felt by the coherently backscattered photons (previously localized). In turn, this latter is a consequence of the enhancement of the effective refractive index near the input border. Therefore, the determination of this internal reflection as a function of the incidence angle is an imperative.

3.3 Backscattering experiment

In order to determine experimentally the effective internal reflection felt by the coherently backscattered photons (*IR*), the intensity of backscattering cone was measured as a function of the incidence angle. Figure 3a, 3b, 3c and 3d show the

backscattering cone, after subtraction of background intensity, for incidence angles of 0º (0 mrad), 30º (524 mrad), 60º (1047 mrad) and 70º (1222 mrad), respectively. The specular reflection measured at the interface silica-sample for the photons that enter the sample is <1% for all incidence angles. From the intensity of the backscattering cone, we extracted the effective internal reflection felt by the coherently backscattered photons (previously localized) at the interface sample-silica (photons coming out the sample). Notice that the backscattering cone must represent those photons previously localized. Figure 3e shows (left-red) the intensity of backscattering cone ($I_{CBC}(\theta)$) and (black-right) *IR* (%) as a function of the incidence angle. We calculated *IR* for each incidence angle, *IR*(θ), by the expression $IR(\theta) = 1 - \frac{I_{CBC}(\theta)}{I^*_{\mathrm{CBC}}}$, where $I_{CBC}(\theta)$ and I^*_{CBC} are the intensity of backscattering cone measured for each incidence angle θ and the ideal intensity for null internal reflection, respectively. The internal reflection for the coherently backscattered photons at normal incidence (*IR*(0º)≈3%) was determined considering an effective refractive index for *depth* near zero of ~2 [16]. From *IR*(0º)≈3%, we can determine I^*_{CBC} and, consequently, *IR*(θ) for the other incidence angles. *IR*(θ) values, determined for θ of 0º, 30º, 60º and 70º are ~3%, ~20%, ~45% and ~65%, respectively, which are considerably higher than the specular reflection measured for the photons that enter the sample (<1%) in the exact opposite direction. This indicates a non-reciprocal propagation of light, i.e. mirror-symmetry (parity symmetry) breaking. Notice that this large increase in the internal reflection undergone by the photons leaving the sample (coherently backscattered) would only be possible if the effective refractive index is largely enhanced. For a classical refractive index (1.53), the internal reflection for the photons leaving the sample (sample-silica interface) would be <1% for both polarizations and all incidence angles. A few pioneering theoretical and experimental studies have addressed the mirror-symmetry breaking in photonic crystal cavities [44–46], however, no experimental evidence has been reported to date in a three-dimensional (3D) disordered optical medium. This phenomenon can be understood as that the photons that enter the sample feel a classical refractive index, but once they are localized; these photons feel an enhanced refractive index due to the successive elastic polarization of valence electrons to virtual states within the localized states.

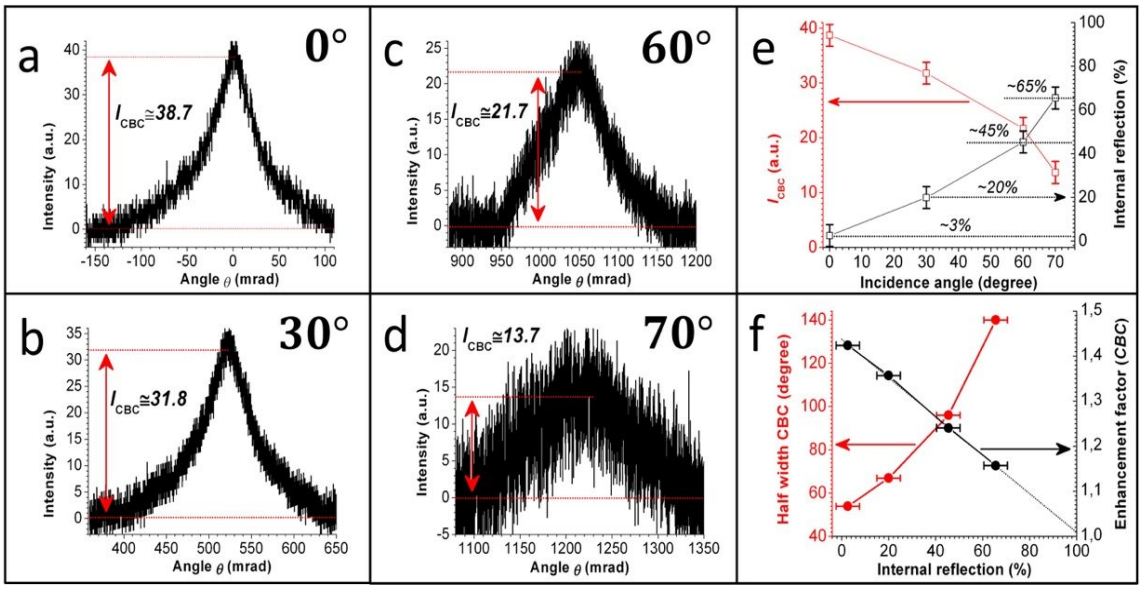

Figure 3. Coherent backscattering cones for incidence angles of: a) 0º, b) 30º, c) 60º and d) 70º. e) (left-red) I_{CBC} and (right-black) *IR* (%) as a function of the incidence angle. f) (left-red) half width of backscattering cone and (right-black) the enhancement factor of backscattering cone as a function of *IR* (%). The black dotted line represents a linear fitting with the experimental points. Error bars correspond to the standard deviation of the intensity of the backscattering cone (I_{CBC}) and the calculated *IR* (%).

Figure 3f shows (left-red) the half width and (black-right) enhancement factor of backscattering cone as a function of the incidence angle. The width of backscattering cone increases monotonically as the incidence angle is increased, which is different to what is expected for a classical diffusive medium where l_{T} is insensitive to the incidence angle. This latter represents a l_{T} decrease as *IR* increases, which indicates an anomalous transport of light. The values of enhancement factor are considerably lower than the expected for a linearly polarized probe beam (~1.8). Additionally, the enhancement factor tends to be 1 for *IR* →100%, which was to be expected. This effect can be explained by: i) the

effective refractive index felt by the coherently backscattered photons (previously localized) is considerably higher than that felt by the incoherently backscattered photons (non-localized photons), which leads to a higher internal reflection for the coherently backscattered photons; ii) the percentage of coherently backscattered photons with orthogonal polarization with regard to the original polarization could increase as the incidence angle is increased. We do not have a clear interpretation for this possible change of polarization. This could be explained by an anomalous nonlinear increase of refractive index, due to the intensity increasing (energy increase) within the localized states during the residence time of localized photons [47]. The latter would give rise to a phase shift that continuously increases during the photon residence time (τ_{eO}). This phase accumulation can lead to interference breaking, emitting photons away from the localized state. This nonlinear increase of the refractive index in a localized state (closed loop path) would provoke an elliptic polarization, much like the Pockels effect. A similar nonlinear phenomenon was theoretically addressed by Buttiker and Moskalets (disordered electronic media) [48], who proposed that when the energy of the localized state changes, the localized state can emit non-equilibrium electrons and holes propagating away from the localized state within the edge state which acts similar to a waveguide. The increase of localization with incidence angle near the input border could be also interpreted as that photons from superficial localized states that would be emitted by nonlinear effects (non-equilibrium) [47,48] can be again trapped in another superficial localized state, due to the increase of internal reflection. This latter implies in that the density and residence time (Q factor) of superficial localized states would increase as internal reflection (incidence angle) increases, which can be inferred from the theoretical predictions of Mirlin [36,18] and Ramos and co-workers [38] in disordered electronic media. Notice that an increase of the internal reflection with the incidence angle would be remarkable, mainly for the coherently backscattered photons (previously localized), due to the enhanced refractive index that these photons would feel. For the incoherently backscattered photons, this effect would be considerably lower, since such photons would feel a classical refractive index.

3.4 Theoretical simulation

We consider the geometry called a "quantum dot" with three point contacts that connect it to three photon reservoirs: first (N1), input terminal; second (N2), transmission terminal and third (N3), backscattering terminal. In order to simulate the size of the scattering region, we use a number of resonances, which is proportional to this size. We consider that the reflection at the input (IR_1) and transmission (IR_2) point contacts are equal zero (IR_1=IR_2=0), i.e. there is no appreciable reflection in the input and output interface. We supposed two different effective internal reflection at the backscattering terminal (N3); an effective internal reflection for the coherently backscattered photons (previously localized photons), IR_{3L}, and another internal reflection for the incoherently backscattered photons (non-localized photons), IR_{3D}. For the incoherently backscattered photons, the internal reflection at the interface sample-silica can be neglected ($IR_{3D}\approx 0$), due to the low contrast between refractive indexes (1.53-1.46). For each effective internal reflection IR_{3L} (backscattering terminal), we computed the conductance from N1 to N2 $\left(\langle g\rangle_{1-2}(IR_{3L})\right)$ as a function of the number of resonances through the equation (4). To this end, we have taken into account the presence (Gaussian orthogonal ensemble (GOE)) or absence (Gaussian unitary ensemble (GUE)) of time-reversal symmetry (TRS).

$$\langle g\rangle_{1-2}(IR_{3L}) = \langle g\rangle_{GOE}(IR_{3L}) - \langle g\rangle_{GUE}(IR_{3L}) + \langle g\rangle_{GUE}(IR_{3D}=0) \quad (4)$$

The terms $\langle g\rangle_{GOE}(IR_{3L})$, $\langle g\rangle_{GUE}(IR_{3L})$ and $\langle g\rangle_{GUE}(IR_{3D}=0)$ represent the conductance from N1 to N2 taking into account: the presence of TRS (IR_{3L}), absence of TRS (IR_{3L}) and absence of TRS with IR_{3D}=0, respectively. The $\langle\cdot\rangle$ symbol denotes the mean in the universal ensembles. The first part of equation (4) $\left(\langle g\rangle_{GOE}(IR_{3L}) - \langle g\rangle_{GUE}(IR_{3L})\right)$ represents the term associated to interference for an effective internal reflection IR_{3L}. Thereby, $\langle g\rangle_{1-2}(IR_{3L})$ is calculated by addition of the unitary term $\langle g\rangle_{GUE}(IR_{3D}=1)$, computed considering an effective internal reflection in N3 equal zero, plus the interferential term, computed by the $\langle g\rangle_{GOE}(IR_{3L}) - \langle g\rangle_{GUE}(IR_{3L})$ expression considering an effective internal reflection IR_{3L}. In short, we have assumed that the coherently backscattered photons (previously localized) feel an effective internal reflection equal to IR_{3L}, while the incoherently backscattered photons (non-localized) feel an effective Internal reflection IR_{3D}=0. In order to compute the conductance at normal incidence, we considered IR_{3L}=3%. Therefore, the asymptotic values (large number of resonances) of relative conductance for each effective internal reflection IR_{3L} $\left(G_{IR_R}(\infty; IR_{3L})\right)$ can be calculated by the equation (5), considering an internal reflection of reference (IR_R) at normal incidence of IR_R=3%.

$$G_{IR_R=3\%}(\infty; IR_{3L}) = \frac{\langle g\rangle_{GOE}(IR_R=3\%) - \langle g\rangle_{GUE}(IR_R=3\%) + \langle g\rangle_{GOE}(IR_{3D}=0)}{\langle g\rangle_{GOE}(IR_{3L}) - \langle g\rangle_{GUE}(IR_{3L}) + \langle g\rangle_{GUE}(IR_{3D}=0)} \quad (5)$$

The $\langle \boldsymbol{g}\rangle$ notation represents the asymptotic values of conductance computed for a great number of resonances. Figure 4 shows $\boldsymbol{G_{IR_R=3\%}(\infty; IR_{3L})}$, computed by theoretical simulation (red dots) and, $G(\infty;\theta)$ (triangles) and $G_{\text{-abs}}(\infty;\theta)$ (open

squares), determined experimentally, as a function of the effective internal reflection IR_{3L} (backscattering terminal). As can be observed, $G(\infty;\theta)$ values for 60º and 70º are lightly higher than $\boldsymbol{G_{IR_R=3\%}(\infty;IR_{3L})}$ values computed by theoretical simulation. This latter can be because the absorption increases appreciably for the incidence angle of 60º and 70º, which provokes an additional decrease of transmitted intensity. However, the theoretical simulation agrees very well with $G_{-abs}(\infty;\theta)$ values determined also experimentally but without the absorption effect, which shows the generality of this approach (random-matrix theory) to address transport phenomena indicating that it does not depend on the sample size or degree of disorder. Additionally, we can infer that the conductance dependence with the incidence angle can be described completely through the transport near the input surface (ergodic regime). The latter could be interpreted such that, the dependence of transport of light with the incidence angle must be determined by those superficial localized states [49], which was previously inferred from the experimental measurements. We must highlight that the number of channels or terminals involved in the propagation experiment ($3x10^3$) is much higher than one considered in the theoretical simulation. Clearly, an increase of the number of terminals must lead to interferences between the terminals, which would affect the conductance value. However, the asymptotic conductance between input and transmission terminals must be scaled by a factor linked to the number of terminals. This factor is canceled mathematically in the calculus of relative conductance. Thereby, the relative conductance must be insensitive to the number of terminals. The relationship between the asymptotic conductance and the number of terminals is beyond the paper scope, which could be a subject for future research. We must clarify that "channel" is a notation commonly used in optics, which would be equivalent to terminals (notation that we have used in the theoretical simulation).

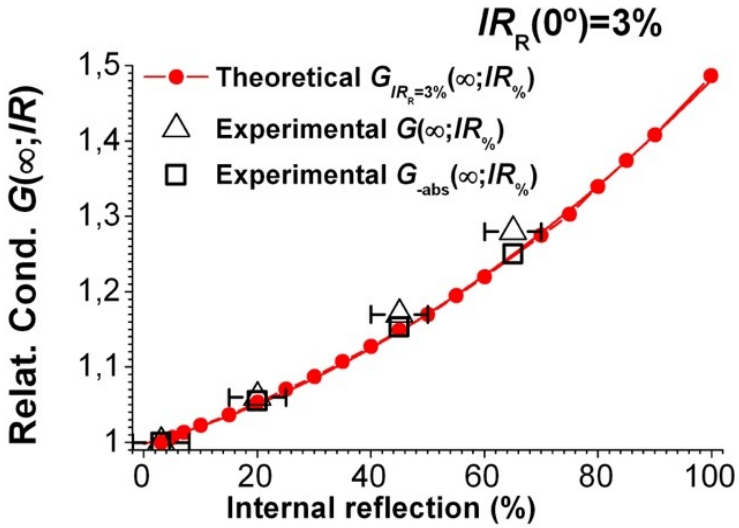

Figure 4. Theoretical and experimental asymptotic values of relative conductance: $\boldsymbol{G_{IR_R=3\%}(\infty;IR_{3L})}$, computed by theoretical simulation (red dots), $\boldsymbol{G(\infty;IR_\%)}$, determined by $\frac{I(0°)}{I(\theta)}$ ratio (black triangles), and $\boldsymbol{G_{-abs}(\infty;IR_\%)}$ without absorption effect, determined by $\frac{I_{Cent}(0°)}{I_{Cent}(\theta)} \times \frac{\omega_{eff}(0°)}{\omega_{eff}(\theta)}$ expression (black squares), as a function of the effective internal reflection felt by the coherently backscattered photons (internal reflection of reference IR_R=3%). Error bars represent the error in determining the effective internal reflection from figure 3e.

4. CONCLUSION

Core–shell TiO_2@Silica nanoparticles allowed us to obtain a liquid suspension with a significantly high scattering strength. A striking phenomenon of enhanced absorption is observed at [NPs]≥$47x10^{10}$ NPs ml^{-1}, which is strong evidence of approaching localization. A Gaussian probe beam that is propagated through the sample at [$140x10^{10}$ NPs ml^{-1}] showed a $e^{-2\left(|r|/\sigma\right)^{1+\nu}}$ ($0<\nu<1$) intensity profile at the sample output, instead of a Gaussian profile. The integrated intensity of the intensity profile shown a decrease as the incidence angle is increased. Additionally, a decrease of the effective width (intensity profile) is observed for angles of incidence of 60º and 70º. However, for [$14x10^{10}$ NPs ml^{-1}] (diffusive regimen), the photon cloud shown a Gaussian profile, whose integrated intensity and effective width are insensitive to the incidence angle. From the experimental results, we inferred that an increase of the internal reflection

(incidence angle) must provoke an increase of the density and residence time (Q factor) of superficial localized states, which is reflected in an increase of localization and absorption near the input border. The specular reflection at the interface silica-sample, measured for the photons that enter the sample, is considerably lower than the effective internal reflection determined for the coherently backscattered photons in the exact opposite direction, which indicates a breaking of the mirror-symmetry (parity symmetry). The relative conductance was computed by random-matrix theory (theoretical simulation) as a function of the effective internal reflection felt by the coherently backscattered photon, revealing a conductance decrease as the effective internal reflection decreases. Theoretical simulation agrees very well with the experimental results, which indicates the generality of random-matrix theory to address the transport phenomena.

ACKNOWLEDGEMENTS

We acknowledge financial support from FACEPE, CNPq and FAPESP (grants 2017 05854-9 and 2017 10765-5).

REFERENCES

[1] Genovese, M. P., Lightcap, I. V. and Kamat, P. V., "Sun-Believable Solar Paint. A Transformative One-Step Approach for Designing Nanocrystalline Solar Cells," ACS Nano **6**(1), 865–872 (2012).

[2] Wetter, N. U., Giehl, J. M., Butzbach, F., Anacleto, D. and Jiménez-Villar, E., "Polydispersed Powders (Nd 3+ :YVO 4) for Ultra Efficient Random Lasers," Part. Part. Syst. Charact., 1700335 (2017).

[3] Vieira, R. J. R., Gomes, L., Martinelli, J. R. and Wetter, N. U., "Upconversion luminescence and decay kinetics in a diode-pumped nanocrystalline Nd^3+:YVO_4 random laser," Opt. Express **20**(11), 12487 (2012).

[4] Jorge, K. C., Alvarado, M. A., Melo, E. G., Carreño, M. N. P., Alayo, M. I. and Wetter, N. U., "Directional random laser source consisting of a HC-ARROW reservoir connected to channels for spectroscopic analysis in microfluidic devices," Appl. Opt. **55**(20), 5393 (2016).

[5] John, S., "Electromagnetic absorption in a disordered medium near a photon mobility edge," Phys. Rev. Lett. **53**(22), 2169–2172 (1984).

[6] Anderson, P. W., "The question of classical localization A theory of white paint?," Philos. Mag. Part B **52**(3), 505–509 (1985).

[7] John, S., "Strong localization of photons in certain disordered dielectric superlattices," Phys. Rev. Lett. **58**(23), 2486–2489 (1987).

[8] John, S., "Localization of Light," Phys. Today **44**(5), 32 (1991).

[9] Wiersma, D. S., Bartolini, P., Lagendijk, A. and Righini, R., "Localization of light in a disordered medium," Nature **390**(6661), 671–673 (1997).

[10] St??rzer, M., Gross, P., Aegerter, C. M. and Maret, G., "Observation of the critical regime near anderson localization of light," Phys. Rev. Lett. **96**(6), 1–4 (2006).

[11] Sperling, T., Bührer, W., Aegerter, C. M. and Maret, G., "Direct determination of the transition to localization of light in three dimensions," Nat. Photonics **7**(1), 48–52 (2013).

[12] Wiersma, D. S., Bartolini, P., Gómez Rivas, J., Lagendijk, A. and Righini, R., "Reply: Localization or classical diffusion of light?," Nature **398**(6724), 181 (1999).

[13] Scheffold, F. and Wiersma, D., "Inelastic scattering puts in question recent claims of Anderson localization of light," Nat. Photonics **7**(12), 934 (2013).

[14] Van Der Beek, T., Barthelemy, P., Johnson, P. M., Wiersma, D. S. and Lagendijk, A., "Light transport through disordered layers of dense gallium arsenide submicron particles," Phys. Rev. B - Condens. Matter Mater. Phys. **85**(11), 1–11 (2012).

[15] Sperling, T., Schertel, L., Ackermann, M., Aubry, G. J., Aegerter, C. M. and Maret, G., "Can 3D light localization be reached in 'white paint'?," New J. Phys. **18**(1), 13039 (2016).

[16] Jimenez-Villar, E., da Silva, I. F., Mestre, V., de Oliveira, P. C., Faustino, W. M. and de Sá, G. F., "Anderson localization of light in a colloidal suspension (TiO 2 @silica)," Nanoscale **8**(21), 10938–10946 (2016).

[17] Al 'tshuler, B. L. and Shklovskii, B. I., "Repulsion of energy levels and conductivity of small metal samples," Sov. Phys. J. Exp. Theor. Phys. **64**(1), 127–135 (1986).

[18] Mirlin, A., "Statistics of energy levels and eigenfunctions in disordered systems," Phys. Rep. **326**(5–6), 259–382 (2000).

[19] Abderrafi, K., Jiménez, E., Ben, T., Molina, S. I., Ibáñez, R., Chirvony, V. and Martínez-Pastor, J. P., "Production of Nanometer-Size GaAs Nanocristals by Nanosecond Laser Ablation in Liquid," J. Nanosci. Nanotechnol. **12**(8), 6774–6778 (2012).

[20] Jimenez-Villar, E., Mestre, V., de Oliveira, P. C. and de Sá, G. F., "Novel core–shell (TiO2@Silica) nanoparticles for scattering medium in a random laser: higher efficiency, lower laser threshold and lower photodegradation," Nanoscale **5**(24), 12512 (2013).
[21] Skipetrov, S. E. and Sokolov, I. M., "Absence of Anderson Localization of Light in a Random Ensemble of Point Scatterers," Phys. Rev. Lett. **112**(2), 23905 (2014).
[22] Jimenez-Villar, E., Mestre, V., de Oliveira, P. C., Faustino, W. M., Silva, D. S. and de Sá, G. F., "TiO 2 @Silica nanoparticles in a random laser: Strong relationship of silica shell thickness on scattering medium properties and random laser performance," Appl. Phys. Lett. **104**(8), 81909 (2014).
[23] Rodriguez, E., Jimenez, E., Jacob, G. J., Neves, A. A. R., Cesar, C. L. and Barbosa, L. C., "Fabrication and characterization of a PbTe quantum dots multilayer structure," Phys. E Low-dimensional Syst. Nanostructures **26**(1–4), 361–365 (2005).
[24] Rodriguez, E., Kellermann, G., Craievich, A. F., Jimenez, E., César, C. L. and Barbosa, L. C., "All-optical switching device for infrared based on PbTe quantum dots," Superlattices Microstruct. **43**(5–6), 626–634 (2008).
[25] Jiménez, E., Abderrafi, K., Abargues, R., Valdés, J. L. and Martínez-Pastor, J. P., "Laser-Ablation-Induced Synthesis of SiO 2 -Capped Noble Metal Nanoparticles in a Single Step," Langmuir **26**(10), 7458–7463 (2010).
[26] Jiménez, E., Abderrafi, K., Martínez-Pastor, J., Abargues, R., Luís Valdés, J. and Ibáñez, R., "A novel method of nanocrystal fabrication based on laser ablation in liquid environment," Superlattices Microstruct. **43**(5–6), 487–493 (2008).
[27] González-Castillo, J. R., Rodriguez, E., Jimenez-Villar, E., Rodríguez, D., Salomon-García, I., de Sá, G. F., García-Fernández, T., Almeida, D. B., Cesar, C. L., Johnes, R. and Ibarra, J. C., "Synthesis of Ag@Silica Nanoparticles by Assisted Laser Ablation," Nanoscale Res. Lett. **10**(1), 399 (2015).
[28] González-Castillo, J. R., Rodríguez-González, E., Jiménez-Villar, E., Cesar, C. L. and Andrade-Arvizu, J. A., "Assisted laser ablation: silver/gold nanostructures coated with silica," Appl. Nanosci. **7**(8), 597–605 (2017).
[29] Ermakov, V. A., Jimenez-Villar, E., Silva Filho, J. M. C. da, Yassitepe, E., Mogili, N. V. V., Iikawa, F., de Sá, G. F., Cesar, C. L. and Marques, F. C., "Size Control of Silver-Core/Silica-Shell Nanoparticles Fabricated by Laser-Ablation-Assisted Chemical Reduction," Langmuir **33**(9), 2257–2262 (2017).
[30] Sánchez-Muñoz, O. L., Salgado, J., Martínez-Pastor, J. and Jiménez-Villar, E., "Synthesis and Physical Stability of Novel Au-Ag@SiO2 Alloy Nanoparticles," Nanosci. Nanotechnol. **2**(1), 1–7 (2012).
[31] Rodríguez, E., Jimenez, E., Padilha, L. A., Neves, A. A. R., Jacob, G. J., César, C. L. and Barbosa, L. C., "SiO2/PbTe quantum-dot multilayer production and characterization," Appl. Phys. Lett. **86**(11), 113117 (2005).
[32] Kellermann, G., Rodriguez, E., Jimenez, E., Cesar, C. L., Barbosa, L. C. and Craievich, A. F., "Structure of PbTe(SiO 2)/SiO 2 multilayers deposited on Si(111)," J. Appl. Crystallogr. **43**(3), 385–393 (2010).
[33] Fuertes, G., Sánchez-Muñoz, O. L., Pedrueza, E., Abderrafi, K., Salgado, J. and Jiménez, E., "Switchable Bactericidal Effects from Novel Silica-Coated Silver Nanoparticles Mediated by Light Irradiation," Langmuir **27**(6), 2826–2833 (2011).
[34] Fuertes, G., Pedrueza, E., Abderrafi, K., Abargues, R., Sánchez, O., Martínez-Pastor, J., Salgado, J. and Jiménez, E., "Photoswitchable bactericidal effects from novel silica-coated silver nanoparticles," Prog. Biomed. Opt. Imaging - Proc. SPIE **8092**, R. Sroka and L. D. Lilge, Eds., 80921M (2011).
[35] Rodríguez, E., Jimenez, E., Cesar, C. L., Barbosa, L. C. and De Araújo, C. B., "1D photonic band gap PbTe doped silica quantum dot optical device," Glas. Technol. **46**(2), 47–49(3) (2005).
[36] Mirlin, A. D., "Spatial structure of anomalously localized states in disordered conductors," J. Math. Phys. **38**(4), 1888–1917 (1997).
[37] Campagnano, G. and Nazarov, Y. V., "G(Q) corrections in the circuit theory of quantum transport," Phys. Rev. B **74**(12), 1–15 (2006).
[38] Barbosa, A. L. R., Bazeia, D. and Ramos, J. G. G. S., "Universal Braess paradox in open quantum dots," Phys. Rev. E **90**(4), 42915 (2014).
[39] Bohigas, O., Giannoni, M. J. and Schmit, C., "Characterization of Chaotic Quantum Spectra and Universality of Level Fluctuation Laws," Phys. Rev. Lett. **52**(1), 1–4 (1984).
[40] Beenakker, C. W. J., "Random-matrix theory of quantum transport," Rev. Mod. Phys. **69**(3), 731–808 (1997).
[41] Imry, Y., "Active Transmission Channels and Universal Conductance Fluctuations," Europhys. Lett. **1**(5), 249–256 (1986).
[42] Jimenez-Villar, E., Mestre, V., Martins, W. S., Basso, G. F., da Silva, I. F. and de Sá, G. F., "Core-shell TiO 2 @Silica nanoparticles for light confinement," Mater. Today Proc. **4**(11), 11570–11579 (2017).
[43] van der Mark, M. B., van Albada, M. P. and Lagendijk, A., "Light scattering in strongly scattering media:

Multiple scattering and weak localization," Phys. Rev. B **37**(7), 3575–3592 (1988).
[44] Maes, B., Bienstman, P. and Baets, R., "Switching in coupled nonlinear photonic-crystal resonators," J. Opt. Soc. Am. B **22**(8), 1778 (2005).
[45] Maes, B., Soljacic, M., Joannopoulos, J. D., Bienstman, P., Baets, R., Gorza, S.-P. and Haelterman, M., "Switching through symmetry breaking in coupled nonlinear micro-cavities," Opt. Express **14**(22), 10678 (2006).
[46] Hamel, P., Haddadi, S., Raineri, F., Monnier, P., Beaudoin, G., Sagnes, I., Levenson, A. and Yacomotti, A. M., "Spontaneous mirror-symmetry breaking in coupled photonic-crystal nanolasers," Nat. Photonics **9**(5), 311–315 (2015).
[47] Jiménez-Villar, E., da Silva, I. F., Mestre, V., Wetter, N. U., Lopez, C., de Oliveira, P. C., Faustino, W. M. and de Sá, G. F., "Random Lasing at Localization Transition in a Colloidal Suspension (TiO 2 @Silica)," ACS Omega **2**(6), 2415–2421 (2017).
[48] Büttiker, M. and Moskalets, M., "FROM ANDERSON LOCALIZATION TO MESOSCOPIC PHYSICS," Int. J. Mod. Phys. B **24**(12n13), 1555–1576 (2010).
[49] Jimenez-Villar, E., Xavier, M. C. S., Mestre, V., Martins, W. S., Basso, G. F., Wetter, N. U. and de Sa, G. F., "Anderson localization of light: Strong dependence with incident angle" (2017).